An Implicit-Explicit Discontinuous Galerkin Scheme using a Newton-Free Picard Iteration for a Thin-Film Model

by

Caleb Logemann

A thesis submitted to the graduate faculty

in partial fulfillment of the requirements for the degree of

MASTER OF SCIENCE

Major: Applied Mathematics

Program of Study Committee:
James Rossmanith, Major Professor
Alric Rothmayer
Jue Yan

The student author, whose presentation of the scholarship herein was approved by the program of study committee, is solely responsible for the content of this dissertation/thesis. The Graduate College will ensure this dissertation/thesis is globally accessible and will not permit alterations after a degree is conferred.

Iowa State University

Ames, Iowa

2019

Contents

Page

List of Tables

List of Figures

ABSTRACT

This paper provides a high-order numerical scheme for solving Thin-Film models of the form $q_t + (q^2 - q^3)_x = -(q^3 q_{xxx})_x$. This numerical scheme is a discontinuous Galerkin method that builds upon the original modal discontinuous Galerkin method as well as the local discontinuous Galerkin method. Propogation in time is done with an Implicit-Explicit Runge Kutta scheme, so as to allow for larger time steps. The timestep restriction for these methods is determined by the hyperbolic wavespeed restriction, and is not limited by the diffusion term. The resulting nonlinear equations are solved with a Newton-Free iteration. In fact the nonlinear system is solved using a Picard Iteration, where very few iterations are required for convergence.

Chapter1. Introduction

In this paper we look at the model equation,

$$q_t + \left(q^2 - q^3\right)_x = -\left(q^3 q_{xxx}\right)_x \quad (x,t) \in [a,b] \times [0,T]. \tag{1.1}$$

This equation describes the motion of a thin film of liquid flowing over a one-dimensional domain, where $q(x,t) \geq 0$ is the height of the liquid. This fluid is acted upon by gravity, by forces on the surface, and by surface tension. An equivalent model can be derived using thermocapillary forces and molecular forces. This model is useful in many different applications including airplane de-icing[**?**,]] and industrial coating. Some experimental study [**?**,]]article:cazabat1990fingering, article:kataoka1997theoretical, article:ludviksson1971dynamics has been done and numerical results have shown good agreement with those experiments in [**?**,]]article:bertozzi1998contact.

Previous numerical methods for this type of equation have focused on finite difference approaches. Bertozzi and Brenner[**?**,]]bertozzi1997linear used a fully implicit centered finite difference scheme to explore instabilities. Ha et al.[**?**,]]article:Ha2008 explored several different finite difference schemes, some fully implicit and some using the Crank-Nicolson method. In their analysis the considered several different methods for the hyperbolic terms including WENO, Godunov, and an adapted Upwind method. All of these methods were limited to just first or second order, and they required solving a Newton iteration. Finite difference methods also lack provable stability.

We chose to use discontinuous Galerkin methods as they allow for high order convergence. The discontinuous Galerkin methods were first introduced by Reed and Hill[**?**,]]techreport:Reed1973, and then were formalized by Cockburn and Shu in a series of papers[**?**,]]article:Cockburn1991I, article:Cockburn1989II, article:Cockburn1989III, article:Cockburn1990IV, article:cockburn1998V. We use the original modal discontinuous Galerkin method as well as the local discontinuous Galerkin method. The local discontinuous Galerkin method was also formulated by Cockburn and Shu[**?**,]]article:Cockburn1998LDG to handle higher order derivatives with the discontinuous Galerkin

method. We use the modal discontinuous Galerkin method to discretize the convection term and the local discontinuous Galerkin method to discretize the diffusion term.

The diffusion term is much stiffer of a problem then the hyperbolic convection. If the diffusion is handled explicitly in time, then a very strict time step restriction is present for stability. Therefore implicit schemes should be preferred. However the hyperbolic term is nonlinear, and so an implicit scheme would require a Newton iteration. Thus we chose to use an Implicit-Explicit Runge Kutta scheme for propagating in time. These schemes were first introduced by Ascher et al.[**?**,]]article:ascher1997implicit and have been expanded on by Kennedy and Carpenter[**?**,]]kennedy2003additive and Pareschi and Russo[**?**,]]article:pareschi2000IMEX.

Chapter2. The Thin-Film Model

In this model we consider a thin film of liquid on a flat surface with a free interface. This liquid is driven by gravity, shear and normal forces on the surface, and surface tension (see Figure 2.1). We begin by considering the two dimensional incompressible Navier-Stokes equations, which have the form,

$$u_x + w_z = 0 \tag{2.1}$$

$$\rho(u_t + uu_x + wu_z) = -p_x + \mu\Delta u - \phi_x \tag{2.2}$$

$$\rho(w_t + uw_x + ww_z) = -p_z + \mu\Delta w - \phi_z \tag{2.3}$$

where ρ is the density, u is the horizontal velocity, w is the vertical velocity, p is the pressure, and ϕ is the force of gravity. Equation (2.1) is the incompressibility condition and also represents conservation of mass. Equations (2.2) and (2.3) represent the conservation of momementum in the x and z directions respectively. We take a no penetration and no slip boundary condition at the lower boundary and the kinimatic boundary condition at the upper boundary. These boundary conditions can be expressed as follows,

$$w = 0, u = 0 \qquad \text{at } z = 0 \tag{2.4}$$

$$w = h_t + uh_x \qquad \text{at } z = h \tag{2.5}$$

where h is the height of the liquid. We can also describe the stress tensor, $\mathbf{T}$, at the free surface, $z = h$, as

$$\mathbf{T} \cdot \mathbf{n} = (-\kappa\sigma + \Pi_0)\mathbf{n} + \left(\frac{\partial\sigma}{\partial s} + \tau_0\right)\mathbf{t} \qquad \text{at } z = h$$

where κ is the mean curvature, σ is the surface tension, and Π_0 and τ_0 are the normal and tangential components of the forcing respectively.

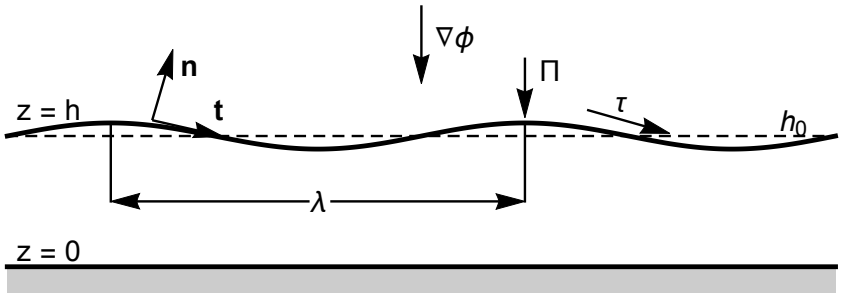

Figure 2.1 A diagram of the situation in question.

These equations completely describe the fluid, but we are now going to make a lubrication approximation, through a scaling argument. For the lubrication approximation we are going to assume that the average height of the liquid, h_0, is much smaller then the characterstic wavelength of the liquid, λ. We will denote the ratio of these two lengths as ε, that is

$$\varepsilon = \frac{h_0}{\lambda} \ll 1. \tag{2.6}$$

Now we nondimensionalize the rest of the variables with respect to this ratio. We denote the nondimensional variables as the uppercase variables. As we stated earlier the characteristic height is h_0 and the characteristic length is $\lambda = h_0/\varepsilon$, so the nondimensional length variables are

$$Z = \frac{z}{h_0}, \quad X = \frac{\varepsilon x}{h_0}, \quad H = \frac{h}{h_0}. \tag{2.7}$$

Let U_0 be the characteristic horizontal velocity, then

$$U = \frac{u}{U_0}, \quad W = \frac{w}{\varepsilon U_0} \tag{2.8}$$

where the nondimensional vertical velocity, W, follows from the continuity equation, equation (2.1). It follows that time will be scaled by λ/U_0, so nondimensional time is

$$T = \frac{\varepsilon U_0 t}{h_0}. \tag{2.9}$$

Finally we assume that the flow is locally parallel or equivalently $p_x \sim \mu u_{zz}$. This gives us the proper scaling for the pressure, gravity, and surface stresses,

$$P = \frac{\varepsilon h_0}{\mu U_0} p, \quad \Phi = \frac{\varepsilon h_0}{\mu U_0}\phi, \quad \Pi = \frac{\varepsilon h_0}{\mu U_0}\Pi_0, \quad \tau = \frac{h_0}{\mu U_0}\tau_0. \tag{2.10}$$

Lastly we can nondimensionalize the surface tension as

$$\Sigma = \frac{\varepsilon\sigma}{\mu U_0} \tag{2.11}$$

The following give some intermediate steps in how to nondimensionalize variables that include derivatives.

$$
\begin{aligned}
u_x &= U_0 U_X \frac{\partial X}{\partial x} = \frac{\varepsilon U_0}{h_0} U_X \\
w_z &= \varepsilon U_0 W_Z \frac{\partial Z}{\partial z} = \frac{\varepsilon U_0}{h_0} W_Z \\
u_t &= U_0 U_T \frac{\partial T}{\partial t} = \frac{\varepsilon U_0^2}{h_0} U_T \\
uu_x &= U_0 U U_0 U_X \frac{\partial X}{\partial x} = \frac{\varepsilon U_0^2}{h_0} U U_X \\
wu_z &= \varepsilon U_0 W U_0 U_Z \frac{\partial Z}{\partial z} = \frac{\varepsilon U_0^2}{h_0} W U_Z \\
w_t &= \varepsilon U_0 W_T \frac{\partial T}{\partial t} = \frac{\varepsilon^2 U_0^2}{h_0} W_T \\
uw_x &= U_0 U \varepsilon U_0 W_X \frac{\partial X}{\partial x} = \frac{\varepsilon^2 U_0^2}{h_0} U W_X \\
ww_z &= \varepsilon U_0 W \varepsilon U_0 W_Z \frac{\partial Z}{\partial z} = \frac{\varepsilon^2 U_0^2}{h_0} W W_Z \\
p_x &= \frac{\mu U_0}{\varepsilon h_0} P_X \frac{\partial X}{\partial x} = \frac{\mu U_0}{h_0^2} P_X \\
p_z &= \frac{\mu U_0}{\varepsilon h_0} P_Z \frac{\partial Z}{\partial z} = \frac{\mu U_0}{\varepsilon h_0^2} P_Z \\
u_{xx} &= U_0 U_{XX} \left(\frac{\partial X}{\partial x} \right)^2 = \frac{\varepsilon^2 U_0}{h_0^2} U_{XX} \\
u_{zz} &= U_0 U_{ZZ} \left(\frac{\partial Z}{\partial z} \right)^2 = \frac{U_0}{h_0^2} U_{ZZ} \\
w_{xx} &= \varepsilon U_0 W_{XX} \left(\frac{\partial X}{\partial x} \right)^2 = \frac{\varepsilon^3 U_0}{h_0^2} W_{XX} \\
w_{zz} &= \varepsilon U_0 U_{ZZ} \left(\frac{\partial Z}{\partial z} \right)^2 = \frac{\varepsilon U_0}{h_0^2} W_{ZZ} \\
\phi_x &= \frac{\mu U_0}{\varepsilon h_0} \Phi_X \frac{\partial X}{\partial x} = \frac{\mu U_0}{h_0^2} \Phi_X \\
\phi_z &= \frac{\mu U_0}{\varepsilon h_0} \Phi_Z \frac{\partial Z}{\partial z} = \frac{\mu U_0}{\varepsilon h_0^2} \Phi_Z \\
h_t &= h_0 H_T \frac{\partial T}{\partial t} = \varepsilon U_0 H_T \\
uh_x &= U_0 U h_0 H_X \frac{\partial X}{\partial x} = \varepsilon U_0 U H_X
\end{aligned}
$$

Substituting these nondimensional variables into the continuity equation (2.1), gives

$$\begin{aligned} u_x + w_z &= 0 \\ \frac{\varepsilon U_0}{h_0} U_X + \frac{\varepsilon U_0}{h_0} W_Z &= 0 \\ U_X + W_Z &= 0 \end{aligned}$$

This computation also justifies the scaling of w as the nondimensional variables should also conserve mass.

We can nondimensionalize the conservation of momementum equations as follows,

$$\begin{aligned} \rho(u_t + uu_x + wu_z) &= -p_x + \mu\Delta u - \phi_x \\ \rho\left(\frac{\varepsilon U_0^2}{h_0} U_T + \frac{\varepsilon U_0^2}{h_0} UU_X + \frac{\varepsilon U_0^2}{h_0} WU_Z\right) &= -\frac{\mu U_0}{h_0^2} P_X + \mu\left(\frac{\varepsilon^2 U_0}{h_0^2} U_{XX} + \frac{U_0}{h_0^2} U_{ZZ}\right) - \frac{\mu U_0}{h_0^2}\Phi_X \\ \frac{\varepsilon U_0^2 \rho}{h_0}(U_T + UU_X + WU_Z) &= \frac{\mu U_0}{h_0^2}\Big(-P_X + \Big(\varepsilon^2 U_{XX} + U_{ZZ}\Big) - \Phi_X\Big) \\ \frac{\varepsilon U_0 \rho h_0}{\mu}(U_T + UU_X + WU_Z) &= \Big(-P_X + \Big(\varepsilon^2 U_{XX} + U_{ZZ}\Big) - \Phi_X\Big) \end{aligned}$$

and

$$\begin{aligned} \rho(w_t + uw_x + ww_z) &= -p_z + \mu\Delta w - \phi_z \\ \rho\left(\frac{\varepsilon^2 U_0^2}{h_0} W_T + \frac{\varepsilon^2 U_0^2}{h_0} UW_X + \frac{\varepsilon^2 U_0^2}{h_0} WW_Z\right) &= -\frac{\mu U_0}{\varepsilon h_0^2} P_Z + \mu\left(\frac{\varepsilon^3 U_0}{h_0^2} W_{XX} + \frac{\varepsilon U_0}{h_0^2} W_{ZZ}\right) - \frac{\mu U_0}{\varepsilon h_0^2}\Phi_Z \\ \frac{\varepsilon^2 \rho U_0^2}{h_0}(W_T + UW_X + WW_Z) &= \frac{\mu U_0}{\varepsilon h_0^2}\Big(-P_Z + \Big(\varepsilon^4 W_{XX} + \varepsilon^2 W_{ZZ}\Big) - \Phi_Z\Big) \\ \varepsilon^3 \frac{\rho U_0 h_0}{\mu}(W_T + UW_X + WW_Z) &= \Big(-P_Z + \varepsilon^2\Big(\varepsilon^2 W_{XX} + W_{ZZ}\Big) - \Phi_Z\Big) \end{aligned}$$

The boundary conditions are nondimensionalized as below,

$$\begin{aligned} w = 0, u = 0 &\qquad \text{at } z = 0 \\ \varepsilon U_0 W = 0, U_0 U = 0 &\qquad \text{at } Z = 0 \\ W = 0, U = 0 &\qquad \text{at } Z = 0 \end{aligned}$$

with

$$w = h_t + uh_x \qquad \text{at } z = h$$

$$\varepsilon U_0 W = \varepsilon U_0 H_T + \varepsilon U_0 U H_x \qquad \text{at } Z = H$$

$$W = H_T + U H_x \qquad \text{at } Z = H$$

In order to nondimensionalize the stress tensor at the free surface, we consider the normal and tangential components of $\mathbf{T} \cdot \mathbf{n}$ separately. The normal and tangential vector at the surface can be expressed in terms of the free surface as

$$\mathbf{n} = \frac{\langle -h_x, 1 \rangle}{(1 + h_x^2)^{1/2}} \quad \mathbf{t} = \frac{\langle 1, h_x \rangle}{(1 + h_x^2)^{1/2}} \tag{2.12}$$

and the mean curvature, κ, can be expressed in terms of h as

$$\kappa = -\frac{h_{xx}}{(1 + h_x^2)^{3/2}}. \tag{2.13}$$

We would now like to write the following vector equation in terms of its normal and tangential components.

$$\mathbf{T} \cdot \mathbf{n} = (-\kappa\sigma + \Pi_0)\mathbf{n} + \left(\frac{\partial \sigma}{\partial s} + \tau_0\right)\mathbf{t} \qquad \text{at } z = h$$

Note that we are using a Newtonian stress tensor which is given by

$$\mathbf{T} = \begin{bmatrix} -p & 0 \\ 0 & -p \end{bmatrix} + \mu \begin{bmatrix} 2u_x & u_z + w_x \\ u_z + w_x & 2w_z \end{bmatrix} \tag{2.14}$$

The normal component of this vector equation is given by

$$\langle \mathbf{T} \cdot \mathbf{n}, \mathbf{n} \rangle = (-\kappa\sigma + \Pi_0) \tag{2.15}$$

First we will simplify the left hand side.

$$
\begin{aligned}
a &= \left(1 + h_x^2\right)^{1/2} \\
\langle \mathbf{T}\cdot\mathbf{n}, \mathbf{n}\rangle &= \frac{1}{a^2}\begin{bmatrix} -h_x & 1 \end{bmatrix}\begin{bmatrix} -p + 2\mu u_x & \mu(u_z + w_x) \\ \mu(u_z + w_x) & -p + 2\mu w_z \end{bmatrix}\begin{bmatrix} -h_x \\ 1 \end{bmatrix} \\
&= \frac{1}{a^2}\begin{bmatrix} -h_x & 1 \end{bmatrix}\begin{bmatrix} -h_x(-p + 2\mu u_x) + \mu(u_z + w_x) \\ -h_x\mu(u_z + w_x) + -p + 2\mu w_z \end{bmatrix} \\
&= \frac{1}{a^2}\Big(h_x^2(-p + 2\mu u_x) - \mu h_x(u_z + w_x) - \mu h_x(u_z + w_x) + -p + 2\mu w_z\Big) \\
&= \frac{1}{a^2}\Big(h_x^2(-p + 2\mu u_x) - 2\mu h_x(u_z + w_x) - p + 2\mu w_z\Big) \\
&= \frac{1}{a^2}\Big(\Big(1 + h_x^2\Big)(-p) + 2\mu\Big(h_x^2 u_x + w_z\Big) - 2\mu h_x(u_z + w_x)\Big) \\
&= -p + \frac{2\mu}{a^2}\Big(\Big(h_x^2 u_x + w_z\Big) - h_x(u_z + w_x)\Big)
\end{aligned}
$$

Next simplify the right hand side.

$$(-\kappa\sigma + \Pi_0) = \frac{h_{xx}}{(1 + h_x^2)^{3/2}}\sigma + \Pi_0$$

This gives the following scalar equation,

$$-p - \Pi_0 + \frac{2\mu}{1 + h_x^2}\Big(\Big(h_x^2 u_x + w_z\Big) - h_x(u_z + w_x)\Big) = \frac{h_{xx}}{(1 + h_x^2)^{3/2}}\sigma. \tag{2.16}$$

The tangential component is given by

$$\langle \mathbf{T}\cdot\mathbf{n}, \mathbf{t}\rangle = \left(\frac{\partial\sigma}{\partial s} + \tau_0\right) \tag{2.17}$$

First simplify the left hand side,

$$\begin{aligned}
\langle \mathbf{T}\cdot\mathbf{n},\mathbf{n}\rangle &= \frac{1}{a^2}\begin{bmatrix}1 & h_x\end{bmatrix}\begin{bmatrix}-p+2\mu u_x & \mu(u_z+w_x)\\ \mu(u_z+w_x) & -p+2\mu w_z\end{bmatrix}\begin{bmatrix}-h_x\\ 1\end{bmatrix}\\
&= \frac{1}{a^2}\begin{bmatrix}1 & h_x\end{bmatrix}\begin{bmatrix}-h_x(-p+2\mu u_x)+\mu(u_z+w_x)\\ -h_x\mu(u_z+w_x)+-p+2\mu w_z\end{bmatrix}\\
&= \frac{1}{a^2}\Big(-h_x(-p+2\mu u_x)+\mu(u_z+w_x)+-h_x^2\mu(u_z+w_x)+h_x(-p+2\mu w_z)\Big)\\
&= \frac{1}{a^2}\Big(-h_x(2\mu u_x)+\mu(u_z+w_x)+-h_x^2\mu(u_z+w_x)+h_x(2\mu w_z)\Big)\\
&= \frac{\mu}{a^2}\Big(2h_x(w_z-u_x)+\Big(1-h_x^2\Big)(u_z+w_x)\Big)
\end{aligned}$$

Next simplify the right hand side

$$\begin{aligned}
\left(\frac{\partial\sigma}{\partial s}+\tau_0\right) &= \frac{\partial\sigma}{\partial x}\frac{\partial x}{\partial s}+\tau_0\\
&= \frac{\partial\sigma}{\partial x}\frac{1}{(1+h_x^2)^{1/2}}+\tau_0
\end{aligned}$$

This gives the following scalar equation.

$$\mu\Big(2h_x(w_z-u_x)+\Big(1-h_x^2\Big)(u_z+w_x)\Big)=\frac{\partial\sigma}{\partial x}\Big(1+h_x^2\Big)^{1/2}+\tau_0\Big(1+h_x^2\Big) \tag{2.18}$$

Lastly we will nondimensionalize these two equations.

$$-p-\pi+\frac{2\mu}{1+h_x^2}\Big(\Big(h_x^2u_x+w_z\Big)-h_x(u_z+w_x)\Big)=\frac{h_{xx}}{(1+h_x^2)^{3/2}}\sigma$$

$$-\frac{\mu U_0}{\varepsilon h_0}P-\frac{\mu U_0}{\varepsilon h_0}\Pi+\frac{2\mu}{1+\varepsilon^2H_X^2}\left(\left(\varepsilon^2H_X^2\frac{\varepsilon U_0}{h_0}U_X+\frac{\varepsilon U_0}{h_0}W_Z\right)-\varepsilon H_X\left(\frac{U_0}{h_0}U_Z+\frac{\varepsilon^2U_0}{h_0}W_X\right)\right)$$
$$=\frac{\varepsilon^2}{h_0}\frac{H_{XX}}{(1+\varepsilon^2H_X^2)^{3/2}}\frac{\mu U_0}{\varepsilon}\Sigma$$

$$\left(-\frac{\mu U_0}{\varepsilon h_0}P-\frac{\mu U_0}{\varepsilon h_0}\Pi+\frac{\varepsilon\mu U_0}{h_0}\frac{2}{1+\varepsilon^2H_X^2}\Big(\Big(\varepsilon^2H_X^2U_X+W_Z\Big)-H_X\Big(U_Z+\varepsilon^2W_X\Big)\Big)\right)$$
$$=\frac{\varepsilon\mu U_0}{h_0}\frac{H_{XX}}{(1+\varepsilon^2H_X^2)^{3/2}}\Sigma$$

$$\left(-\frac{\mu U_0}{\varepsilon h_0}P-\frac{\mu U_0}{\varepsilon h_0}\Pi+\frac{\varepsilon\mu U_0}{h_0}\frac{2}{1+\varepsilon^2H_X^2}\Big(\Big(\varepsilon^2H_X^2U_X+W_Z\Big)-H_X\Big(U_Z+\varepsilon^2W_X\Big)\Big)\right)$$
$$=\frac{\varepsilon\mu U_0}{h_0}\frac{H_{XX}}{(1+\varepsilon^2H_X^2)^{3/2}}\Sigma$$

$$\frac{\mu U_0}{\varepsilon h_0}\left(-P-\Pi+\frac{2\varepsilon^2}{1+\varepsilon^2H_X^2}\Big(\Big(\varepsilon^2H_X^2U_X+W_Z\Big)-H_X\Big(U_Z+\varepsilon^2W_X\Big)\Big)\right)=\frac{\mu U_0}{\varepsilon h_0}\frac{\varepsilon^2H_{XX}}{(1+\varepsilon^2H_X^2)^{3/2}}\Sigma$$

$$\left(-P-\Pi+\frac{2\varepsilon^2}{1+\varepsilon^2H_X^2}\Big(\Big(\varepsilon^2H_X^2U_X+W_Z\Big)-H_X\Big(U_Z+\varepsilon^2W_X\Big)\Big)\right)=\frac{\varepsilon^2H_{XX}}{(1+\varepsilon^2H_X^2)^{3/2}}\Sigma$$

and

$$\mu\Big(2h_x(w_z-u_x)+\Big(1-h_x^2\Big)(u_z+w_x)\Big)=\frac{\partial\sigma}{\partial x}\Big(1+h_x^2\Big)^{1/2}+\tau_0\Big(1+h_x^2\Big)$$

$$\mu\left(2\varepsilon H_X\left(\frac{\varepsilon U_0}{h_0}W_Z-\frac{\varepsilon U_0}{h_0}U_X\right)+\Big(1-\varepsilon^2H_X^2\Big)\left(\frac{U_0}{h_0}U_Z+\frac{\varepsilon^2U_0}{h_0}W_X\right)\right)$$
$$=\frac{\mu U_0}{h_0}\Sigma_X\Big(1+\varepsilon^2H_X^2\Big)^{1/2}+\frac{\mu U_0}{h_0}\tau\Big(1+\varepsilon^2H_X^2\Big)$$

$$\frac{\mu U_0}{h_0}\Big(2\varepsilon^2H_X(W_Z-U_X)+\Big(1-\varepsilon^2H_X^2\Big)\Big(U_Z+\varepsilon^2W_X\Big)\Big)$$
$$=\frac{\mu U_0}{h_0}\Big(\Sigma_X\Big(1+\varepsilon^2H_X^2\Big)^{1/2}+\tau\Big(1+\varepsilon^2H_X^2\Big)\Big)$$

$$2\varepsilon^2H_X(W_Z-U_X)+\Big(1-\varepsilon^2H_X^2\Big)\Big(U_Z+\varepsilon^2W_X\Big)$$
$$=\Sigma_X\Big(1+\varepsilon^2H_X^2\Big)^{1/2}+\tau\Big(1+\varepsilon^2H_X^2\Big)$$

The full nondimensional equations are thus

$$U_X + W_Z = 0 \tag{2.19}$$

$$\frac{\varepsilon U_0 \rho h_0}{\mu}(U_T + UU_X + WU_Z) = -P_X + \Big(\varepsilon^2 U_{XX} + U_{ZZ}\Big) - \Phi_X \tag{2.20}$$

$$\varepsilon^3 \frac{\rho U_0 h_0}{\mu}(W_T + UW_X + WW_Z) = -P_Z + \varepsilon^2\Big(\varepsilon^2 W_{XX} + W_{ZZ}\Big) - \Phi_Z \tag{2.21}$$

at $Z = 0$

$$W = 0, \quad U = 0 \tag{2.22}$$

and at $Z = H$

$$W = H_T + UH_x \tag{2.23}$$

$$-P - \Pi + \frac{2\varepsilon^2}{1+\varepsilon^2 H_X^2}\Big(\Big(\varepsilon^2 H_X^2 U_X + W_Z\Big) - H_X\Big(U_Z + \varepsilon^2 W_X\Big)\Big) = \frac{\varepsilon^2 H_{XX}}{\left(1+\varepsilon^2 H_X^2\right)^{3/2}}\Sigma \tag{2.24}$$

$$2\varepsilon^2 H_X(W_Z - U_X) + \Big(1 - \varepsilon^2 H_X^2\Big)\Big(U_Z + \varepsilon^2 W_X\Big) = \Sigma_X\Big(1+\varepsilon^2 H_X^2\Big)^{1/2} + \tau\Big(1+\varepsilon^2 H_X^2\Big) \tag{2.25}$$

We can now let $\varepsilon \to 0$ which results in

$$U_X + W_Z = 0 \tag{2.26}$$

$$P_X + \Phi_X = U_{ZZ} \tag{2.27}$$

$$P_Z + \Phi_Z = 0 \tag{2.28}$$

at $Z = 0$,

$$W = 0, \quad U = 0 \tag{2.29}$$

$$\tag{2.30}$$

and at $Z = H$

$$W = H_T + UH_x \tag{2.31}$$

$$-P - \Pi = \bar{\Sigma} H_{XX} \tag{2.32}$$

$$U_Z = \Sigma_X + \tau \tag{2.33}$$

Note that we assume that the surface tension is large, so that $\bar{\Sigma} = \varepsilon^2\Sigma = O(1)$. This is important in order to keep surface tension effects in the final equation.

Next we integrate the continuity equation over Z.

$$\begin{aligned}
\int_0^H U_X + W_Z \,\mathrm{d}Z &= 0 \\
\int_0^H U_X \,\mathrm{d}Z + W|_{Z=0}^H &= 0 \\
\int_0^H U_X \,\mathrm{d}Z + H_T + UH_X &= 0 \\
H_T + \int_0^H U_X \,\mathrm{d}Z + UH_X &= 0 \\
H_T + \frac{\partial}{\partial X}\left(\int_0^H U \,\mathrm{d}Z\right) &= 0
\end{aligned}$$

Using the boundary conditions we can solve for an expression of U as follows

$$\begin{aligned}
\int_Z^H U_{ZZ} \,\mathrm{d}Z &= \int_Z^H P_X + \Phi_X \,\mathrm{d}Z \\
U_Z|_Z^H &= (P_X + \Phi_X)(H - Z) \\
(\tau + \Sigma_X) - U_Z &= (P_X + \Phi_X)(H - Z) \\
\int_0^Z (\tau + \Sigma_X) - U_Z \,\mathrm{d}Z &= \int_0^Z (P_X + \Phi_X)(H - Z) \,\mathrm{d}Z \\
(\tau + \Sigma_X)Z - U|_{Z=0}^Z &= (P_X + \Phi_X)\left(HZ - \frac{1}{2}Z^2\right) \\
(\tau + \Sigma_X)Z - U &= (P_X + \Phi_X)\left(HZ - \frac{1}{2}Z^2\right) \\
U &= (\tau + \Sigma_X)Z + (P_X + \Phi_X)\left(\frac{1}{2}Z^2 - HZ\right)
\end{aligned}$$

The boundary conditions also give an expression for $P + \Phi$,

$$\begin{aligned}
P_Z + \Phi_Z &= 0 \\
\int_Z^H P_Z + \Phi_Z \,\mathrm{d}Z &= 0 \\
P|_{Z=H} - P + \Phi|_{Z=H} - \Phi &= 0 \\
-\Pi - \bar{\Sigma}H_{XX} - P + \Phi|_{Z=H} - \Phi &= 0 \\
P + \Phi &= \Phi|_{Z=H} - \Pi - \bar{\Sigma}H_{XX}
\end{aligned}$$

Plugging both of these into the integrated continuity equation gives,

$$\begin{aligned}
H_T + \frac{\partial}{\partial X}\left(\int_0^H U \,\mathrm{d}Z\right) &= 0 \\
H_T + \frac{\partial}{\partial X}\left(\int_0^H (\tau + \Sigma_X)Z + (P_X + \Phi_X)\Big(\frac{1}{2}Z^2 - HZ\Big)\,\mathrm{d}Z\right) &= 0 \\
H_T + \left(\frac{1}{2}(\tau + \Sigma_X)H^2 + (P_X + \Phi_X)\Big(\frac{1}{6}H^3 - \frac{1}{2}H^3\Big)\right)_X &= 0 \\
H_T + \left(\frac{1}{2}(\tau + \Sigma_X)H^2 - \frac{1}{3}(P + \Phi)_X H^3\right)_X &= 0 \\
H_T + \left(\frac{1}{2}(\tau + \Sigma_X)H^2 - \frac{1}{3}\Big(\Phi|_{Z=H} - \Pi - \bar{\Sigma}H_{XX}\Big)_X H^3\right)_X &= 0 \\
H_T + \left(\frac{1}{2}(\tau + \Sigma_X)H^2 - \frac{1}{3}(\Phi|_{Z=H} - \Pi)_X H^3\right)_X &= -\Big(\bar{\Sigma}H^3 H_{XXX}\Big)_X
\end{aligned}$$

This is our final Thin Film equation and taking all of the constants to be one gives

$$H_T + \Big(H^2 - H^3\Big)_X = -\Big(H^3 H_{XXX}\Big)_X \tag{2.34}$$

Chapter3. Numerical Methods

3.1 IMEX Runge Kutta Scheme

The Thin-Film model we are trying to solve is a very stiff equation due to the high order derivatives. In order to take reasonable timesteps despite this stiffness we use Implicit Explicit (IMEX) Runge Kutta schemes to propogate our solution through time. The IMEX Runge Kutta scheme propogates time for ordinary differential equations of the form

$$q_t = F(t,q) + G(t,q), \tag{3.1}$$

where F is solely handled explicitly, but G needs to be solved implicitly. A single step of the Runge Kutta IMEX scheme is computed as follows,

$$q^{n+1} = q^n + \Delta t \sum_{i=1}^{s} \left(b'_i F(t_i, u_i)\right) + \Delta t \sum_{i=1}^{s} \left(b_i G(t_i, u_i)\right) \tag{3.2}$$

$$u_i = q^n + \Delta t \sum_{j=1}^{i-1} \Big(a'_{ij} F(t_j, u_j)\Big) + \Delta t \sum_{j=1}^{i} \left(a_{ij} G(t_j, u_j)\right) \tag{3.3}$$

$$t_i = t^n + c_i \Delta t \tag{3.4}$$

where the coefficients a_{ij}, b_i, c_i, a'_{ij}, b'_i, and c'_i are set in the double Butcher tableau

$$\begin{array}{c|c} c' & a' \\ \hline & b'^T \end{array} \qquad \begin{array}{c|c} c & a \\ \hline & b^T \end{array}.$$

Specifically we used the IMEX Schemes first introduced by Pareschi and Russo in [**?**,]]article:pareschi2000IMEX, article:pareschi2005IMEX. The double Butcher tableaus for the 1st, 2nd and 3rd order schemes are given below,

$$\begin{array}{c|c} 0 & 0 \\ \hline & 1 \end{array} \qquad \begin{array}{c|c} 1 & 1 \\ \hline & 1 \end{array}$$

$$\begin{array}{c|ccc} 0 & 0 & 0 & 0 \\ 0 & 0 & 0 & 0 \\ 1 & 0 & 1 & 0 \\ \hline & 0 & \frac{1}{2} & \frac{1}{2} \end{array} \qquad \begin{array}{c|ccc} \frac{1}{2} & \frac{1}{2} & 0 & 0 \\ 0 & -\frac{1}{2} & \frac{1}{2} & 0 \\ 1 & 0 & \frac{1}{2} & \frac{1}{2} \\ \hline & 0 & \frac{1}{2} & \frac{1}{2} \end{array}$$

$$\begin{array}{c|cccc} 0 & 0 & 0 & 0 & 0 \\ 0 & 0 & 0 & 0 & 0 \\ 1 & 0 & 1 & 0 & 0 \\ \frac{1}{2} & 0 & \frac{1}{4} & \frac{1}{4} & 0 \\ \hline & 0 & \frac{1}{6} & \frac{1}{6} & \frac{2}{3} \end{array} \qquad \begin{array}{c|cccc} \alpha & \alpha & 0 & 0 & 0 \\ 0 & -\alpha & \alpha & 0 & 0 \\ 1 & 0 & 1-\alpha & \alpha & 0 \\ \frac{1}{2} & \beta & \eta & \zeta & \alpha \\ \hline & 0 & \frac{1}{6} & \frac{1}{6} & \frac{2}{3} \end{array}$$

$$\alpha = 0.24169426078821$$

$$\beta = 0.06042356519705$$

$$\eta = 0.1291528696059$$

$$\zeta = \frac{1}{2} - \beta - \eta - \alpha$$

For our thin-film model F and G will be the spatial discretizations of the convection and diffusive terms respectively, that is

$$F(t,q) = -\left(q^2 - q^3\right)_x \tag{3.5}$$

$$G(t,q) = -\left(q^3 q_{xxx}\right)_x. \tag{3.6}$$

Since G is the stiffest part of our model, we would like to handle this term implicitly so that our time step is less restricted. Also handling F explicitly allows us to more easily capture the nonlinear behavior.

3.2 Space Discretization

We chose to use the Discontinuous Galerkin Method to discretize our equation in space. First let $\left\{x_{j+1/2}\right\}_0^N$ partition the domain, $[a,b]$, and denote each interval as $I_j = \left[x_{j-1/2}, x_{j+1/2}\right]$ with

$\Delta x_j = x_{j+1/2} - x_{j-1/2}$. The Discontinuous Galerkin solution then exists in the following finite dimensional space,

$$V_h^k = \Big\{ v \in L^1([a,b]) : v|_{I_j} \in P^k(I_j), j = 1, \ldots, N \Big\}, \tag{3.7}$$

where $P^k(I_j)$ denotes the set of polynomials of degree k or less on I_j.

3.2.1 Modal Discontinuous Galerkin

First we consider the continuous operator $F(t,q) = -\left(q^2 - q^3\right)_x$. Note that $F : [0,T] \times C^1(a,b) \to C^0(a,b)$, and we would like to form an approximation, F_h to this continuous operator, such that $F_h : [0,T] \times V_h^k \to V_h^k$. In order to do this, consider the weak formulation of the continuous operator, F. The weak form requires finding $F(t,q) \in C^0(a,b)$ such that

$$\int_a^b F(t,q)v(x)\,\mathrm{d}x = -\int_a^b \Big(q^2 - q^3\Big)_x v(x)\,\mathrm{d}x \tag{3.8}$$

for all smooth functions, $v \in C^\infty(a,b)$. The discontinuous Galerkin approximation is formed by replacing these function spaces with the DG space, V_h^k. This gives that the weak formulation of the approximation F_h is to find $F_h(t,q_h) \in V_h^k$ such that

$$\int_a^b F_h(t,q_h)v_h(x)\,\mathrm{d}x = -\int_a^b \Big(q_h^2 - q_h^3\Big)_x v_h(x)\,\mathrm{d}x \tag{3.9}$$

for all $v_h \in V_h^k$. Using integration by parts this is equivalent to finding $F_h(t,q_h) \in V_h^k$ such that

$$\begin{aligned}\int_{I_j} F_h(t,q_h)v_h(x)\,\mathrm{d}x = &\int_{I_j} \Big(q_h^2 - q_h^3\Big)v_h'(x)\,\mathrm{d}x \\ &- \hat{f}(q_h)_{j+1/2} v_h(x_{j+1/2}) + \hat{f}(q_h)_{j-1/2} v_h(x_{j-1/2})\end{aligned} \tag{3.10}$$

for $j = 1, \ldots, N$ and for all $v_h \in V_h^k$. Since q_h is discontinuous at the cell interfaces $x_{j\pm1/2}$, some numerical flux $\hat{f}$ must be chosen.

We chose to use the Local Lax-Friedrich's numerical flux, that is

$$\hat{f}(q_l, q_r) = \frac{1}{2}(f(q_l) + f(q_r) - \lambda_{max}(q_r - q_l)) \tag{3.11}$$

where f is the flux function, q_l and q_r and the left and right states at the interface, and λ_{max} is the locally maximum wavespeed, that is

$$\lambda_{max} = \max_{q \in [\min\{q_l, q_r\}, \max\{q_l, q_r\}]} \{f'(q)\} \tag{3.12}$$

In our case $f(q) = q^2 - q^3$ and at the interface $x_{j+1/2}$, $q_l = q_h^-(x_{j+1/2})$ and $q_r = q_h^+(x_{j+1/2})$.

3.2.2 Local Discontinuous Galerkin Scheme

Next we look at the continuous operator $G(t, q) = -(q^3 q_{xxx})_x$. In discretizing this operator we follow Local Discontinuous Galerkin (LDG) method first introduced by Cockburn and Shu in [**?**,]]article:Cockburn1998LDG for convection-diffusion systems. We first introduce three auxilliary variables, r, s, u, and rewrite the equation as the following system,

$$r = q_x \tag{3.13}$$

$$s = r_x \tag{3.14}$$

$$u = s_x \tag{3.15}$$

$$G(t, q) = -\Big(q^3 u\Big)_x. \tag{3.16}$$

The weak form of this system is solved by finding functions r, s, u, G such that

$$\int_a^b r(x) w(x)\, \mathrm{d}x = \int_a^b q_x(x) w(x)\, \mathrm{d}x \tag{3.17}$$

$$\int_a^b s(x) y(x)\, \mathrm{d}x = \int_a^b r_x(x) y(x)\, \mathrm{d}x \tag{3.18}$$

$$\int_a^b u(x) z(x)\, \mathrm{d}x = \int_a^b s_x(x) z(x)\, \mathrm{d}x \tag{3.19}$$

$$\int_a^b G(t, q) v(x)\, \mathrm{d}x = -\int_a^b \Big(q^3(x) u(x)\Big)_x v(x)\, \mathrm{d}x \tag{3.20}$$

for all smooth functions $w, y, z, v \in C^\infty(a, b)$. The LDG method arrives from applying the standard DG method to each of these equations. That is we replace the continuous function spaces with the discontinuous finite dimensional DG space, V_h^k. The approximate operator G_h becomes the process of finding $r_h, s_h, u_h, G_h(t, q_h) \in V_h$ such that for all test functions $v_h, w_h, y_h, z_h \in V_h$ the following

equations are satisfied

$$\int_a^b r_h w_h \,\mathrm{d}x = \int_a^b (q_h)_x w_h \,\mathrm{d}x \tag{3.21}$$

$$\int_a^b s_h y_h \,\mathrm{d}x = \int_a^b (r_h)_x y_h \,\mathrm{d}x \tag{3.22}$$

$$\int_a^b u_h z_h \,\mathrm{d}x = \int_a^b (s_h)_x z_h \,\mathrm{d}x \tag{3.23}$$

$$\int_a^b G_h(t, q_h) v_h \,\mathrm{d}x = -\int_a^b \left(q_h^3 u_h\right)_x v_h \,\mathrm{d}x \tag{3.24}$$

given t and $q_h \in V_h^k$. This is equivalent to the following equations for all j, if we use integration by parts,

$$\int_{I_j} r_h w_h \,\mathrm{d}x = \left(\left(\hat{q}_h w_h^-\right)_{j+1/2} - \left(\hat{q}_h w_h^+\right)_{j-1/2}\right) - \int_{I_j} q_h (w_h)_x \,\mathrm{d}x \tag{3.25}$$

$$\int_{I_j} s_h y_h \,\mathrm{d}x = \left(\left(\hat{r}_h y_h^-\right)_{j+1/2} - \left(\hat{r}_h y_h^+\right)_{j-1/2}\right) - \int_{I_j} r_h (y_h)_x \,\mathrm{d}x \tag{3.26}$$

$$\int_{I_j} u_h z_h \,\mathrm{d}x = \left(\left(\hat{s}_h z_h^-\right)_{j+1/2} - \left(\hat{s}_h z_h^+\right)_{j-1/2}\right) - \int_{I_j} s_h (z_h)_x \,\mathrm{d}x \tag{3.27}$$

$$\int_{I_j} G_h(t, q_h) v_h \,\mathrm{d}x = -\left(\left(\widehat{q^3 u_h} v_h^-\right)_{j+1/2} - \left(\widehat{q^3 u_h} v_h^+\right)_{j-1/2}\right) + \int_{I_j} q_h^3 u_h (v_h)_x \,\mathrm{d}x \tag{3.28}$$

where $\hat{q}, \hat{r}, \hat{s}, \widehat{q^3 u}$ are suitably chosen numerical fluxes. A common choice of numerical fluxes are the so-called alternating fluxes, shown below

$$\hat{q}_h = q_h^- \tag{3.29}$$

$$\hat{r}_h = r_h^+ \tag{3.30}$$

$$\hat{s}_h = s_h^- \tag{3.31}$$

$$\widehat{q^3 u}_h = \left(q^3 u\right)_h^+. \tag{3.32}$$

These numerical fluxes are one-sided fluxes that alternate sides for each derivative. They are chosen to make this method stable, and they also allow for the auxilliary variables to be locally solved in terms of q_h, hence where the Local DG method gets its name.

3.3 Nonlinear Solver

Using these discretizations in the Runge Kutta IMEX scheme, requires solving the nonlinear system,

$$u_i - \Delta t a_{ii} G_h(t_i, u_i) = q^n + \Delta t \sum_{j=1}^{i-1} \left(a'_{ij} F_h(t_j, u_j) \right) + \Delta t \sum_{j=1}^{i-1} \left(a_{ij} G_h(t_j, u_j) \right). \tag{3.33}$$

for u_i. The standard approach to solving this system would be to use a Newton iteration, however that would require the Jacobian of the operator $I - \Delta t a_{ii} G_h$, which would be relatively intractable. Therefore we chose to linearize this operator and use a Picard iteration instead, which does not require the Jacobian.

Suppose we are trying to solve the nonlinear equation $L(u) = b$, where $L'(v, u)$ is the nonlinear operator linearized about v acting on u. The Picard iteration for solving this nonlinear equation starts with some initial guess u_0. The next solution is found by solving the following linear problem,

$$L'(u_i, u_{i+1}) = b. \tag{3.34}$$

In other words the next iteration is found by solving the problem linearized about the the previous iteration.

We linearize the operator $G_h(t, q_h)$ by first linearizing $G(t, q)$. The continuous operator linearized about v is given by

$$G'(v, t, q) = -\left(v^3 q_{xxx} \right)_x. \tag{3.35}$$

The linearized discrete operator is now just the LDG method applied to this linearized continuous operator.

We find that the Picard iteration approach provides good results with relatively few iterations. In fact in Section 4 we show that we can achieve first, second, and third order accuracy with only one, two, and three iterations respectively per stage. This approach is much more tractable than a Newton iteration and it converges quickly to the nonlinear solution.

Chapter4. Results

4.1 Manufactured Solution

In order to confirm the order of accuracy of our method, we use the method of manufactured solutions. The method of manufactured solutions picks an exact solution $\hat{q}$ and then adds a source term to the initial partial differential equation to make $\hat{q}$ the true solution to the new differential equation. So we actually solve

$$q_t + \left(q^2 - q^3\right)_x = -\left(q^3 q_{xxx}\right)_x + s \tag{4.1}$$

where

$$s = \hat{q}_t + \left(\hat{q}^2 - \hat{q}^3\right)_x + \left(\hat{q}^3 \hat{q}_{xxx}\right)_x. \tag{4.2}$$

This new PDE's exact solution is now $\hat{q}$. We chose

$$\hat{q} = 0.1 \times \sin(2\pi/20.0 \times (x - t)) + 0.15 \tag{4.3}$$

on $x \in [0, 40]$ with periodic boundary conditions to be our manufactured solution. This manufactued solution is chosen so that our flux $q^2 - q^3$ is in it's convex region.

We solve this problem until $t = 5.0$ with constant, linear, and quadratic basis polynomials. The time step size for these simulations is determined by the Courant–Friedrichs–Lewy (CFL) condition. The CFL condition states that

$$\Delta t = \nu \frac{\Delta x}{\lambda} \tag{4.4}$$

where λ is the wavespeed and ν is the CFL number. For hyperbolic problems solved with explicit Runge Kutta time-stepping, ν, typically follows the pattern $\frac{1}{2n-1}$ where n is the order of the method. For this example the wavespeed is 1, and the timestep is chosen just smaller then the typical CFL number. Specifically the timesteps were $\Delta t = 0.9\Delta x$, $\Delta t = 0.2\Delta x$, and $\Delta t = 0.1\Delta x$ for first, second and third order respectively.

Table 4.1 shows the error for each simulation as the mesh is refined. The table also shows the rate of convergence to the true solution, and in each case the rate of convergence approaches the expected order. Note that the first, second, and third order methods only require one, two, and three Picard iterations respectively. The error is computed in the L^2 sense. First if the numerical solution is in the space V_h^k, then the exact solution is projected onto the space V_h^{k+1}. Let $\hat{q}_h$ be this projection, and we will also project the numerical solution, q_h, onto the space V_h^{k+1} with the same basis. Let $\{\phi_i\}_{i=1}^{N(k+1)}$ be that basis for V_h^{k+1}, then there exists coefficients, $\hat{Q}_i$ and Q_i, such that

$$\hat{q}_h = \sum_{i=1}^{N(k+1)} \left(\hat{Q}_i \phi_i(x)\right) \text{ and } q_h = \sum_{i=1}^{N(k+1)} \left(Q_i \phi_i(x)\right). \tag{4.5}$$

The error is then computed as

$$e_N = \sqrt{\frac{\sum_{i=1}^{N(k+1)} \left(\hat{Q}_i - Q_i\right)^2}{\sum_{i=1}^{N(k+1)} \left(\hat{Q}_i^2\right)}}. \tag{4.6}$$

This is equivalent to leading order to

$$e = \sqrt{\int_a^b (\hat{q} - q_h)^2 \, \mathrm{d}x}. \tag{4.7}$$

The order of convergence is then computed from these errors as

$$\text{order} = \log_2\left(\frac{e_N}{e_{2N}}\right). \tag{4.8}$$

Table 4.2 shows how the error is affected when the number of Picard iterations is decreased.

4.2 Traveling Waves

In this section we showcase several numerical examples that demonstrate the traveling wave profiles of equation (1.1). The traveling wave profiles differ from the standard hyperbolic wave profile in several ways. They differ in that they may not be unique and may include undercompressive shocks. These examples were first shown in [**?**,]]article:Bertozzi1999 with first order accuracy.

In these examples, we use a moving reference frame to keep the mesh size reasonable. This is done by actually simulating the following equation,

$$q_t + \left(q^2 - q^3 - sq\right)_x = -\left(q^3 q_{xxx}\right)_x \tag{4.9}$$

	1st Order		2nd Order		3rd Order	
n	error	order	error	order	error	order
20	0.136	—	7.34×10^{-3}	—	5.29×10^{-4}	—
40	0.0719	0.91	1.99×10^{-3}	1.89	5.38×10^{-5}	3.30
80	0.0378	0.93	5.60×10^{-4}	1.83	7.47×10^{-6}	2.85
160	0.0191	0.99	1.56×10^{-4}	1.85	9.97×10^{-7}	2.91
320	0.00961	0.99	3.98×10^{-5}	1.97	1.26×10^{-7}	2.98
640	0.00483	0.99	1.00×10^{-5}	1.99	1.58×10^{-8}	3.00
1280	0.00242	1.00	2.50×10^{-6}	2.00	1.98×10^{-9}	3.00

Table 4.1 Convergence table with a constant, linear, quadratic polynomial bases. Nonlinear solve uses one, two, or three Picard iterations respectively. CFL = 0.9, 0.2, 0.1 respectively

	1 Iteration		2 Iterations		3 Iterations	
n	error	order	error	order	error	order
20					5.29×10^{-4}	—
40					5.38×10^{-5}	3.30
80					7.47×10^{-6}	2.85
160					9.97×10^{-7}	2.91
320					1.26×10^{-7}	2.98
640					1.58×10^{-8}	3.00

Table 4.2 Convergence table with a quadratic polynomial basis. One, Two, and Three Picard iterations are used for each nonlinear solve. CFL = 0.1

where s is the Rankine-Hugoniot wavespeed of the original numerical flux, f

$$s = \frac{f(q_l) - f(q_r)}{q_l - q_r} = q_l + q_r - (q_l^2 + q_l q_r + q_r^2). \tag{4.10}$$

This modified equation will have zero wavespeed in most cases and simulates the original PDE in a moving reference frame.

These examples consider Riemann Problems with different left and right states. Depending on the left and right states they are several different wave profiles. For these examples we will fix the right state and vary the left state. The wave profiles would be qualitatively equivalent for different values for the right state, however the values of the left state would also need to change accordingly.

4.2.0.1 Case 1: Unique Weak Lax Shock

Consider a Riemann Problem with left state, $q_l = 0.3$, and right state, $q_r = 0.1$. We will use the following smoothed out profile as an initial condition for this problem

$$q_0(x) = (\tanh(-x) + 1)\frac{q_l - q_r}{2} + q_r \tag{4.11}$$

For this initial condition the numerical solution approaches a steady wave profile with a unique Lax type shock. Figure 4.1 shows a plot of the solution with this initial condition after enough time for the solution to hit its steady state. Note that this behavior persists for all q_l up to some bound which depends on q_r.

4.2.0.2 Case 2: Multiple Lax Shocks

If the left state is increased to $q_l = 0.3323$, then the wave profile is no longer unique. In this case the steady traveling wave depends on the initial conditions.

For the following initial conditions,

$$q_0(x) = (\tanh(-x) + 1)\frac{q_l - q_r}{2} + q_r \tag{4.12}$$

the behavior is the same as in case 1. The numerical solution for this initial condition is shown in Figure 4.2

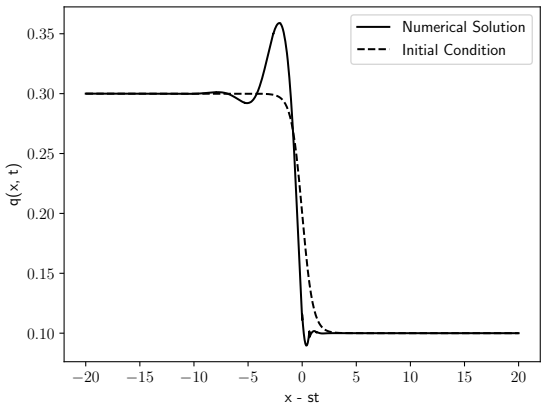

Figure 4.1 Case 1: Unique Lax Shock

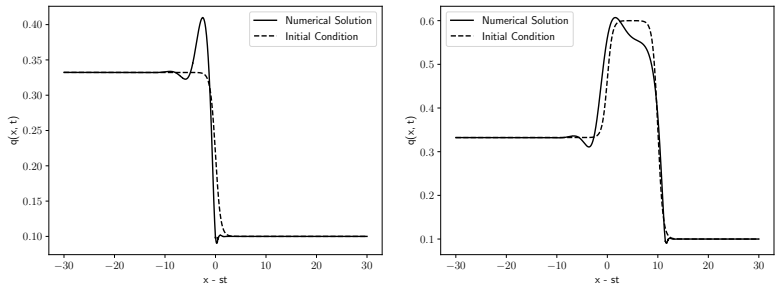

Figure 4.2 Case 2: Multiple Lax Shocks

Now consider the following initial conditions,

$$q_0(x) = \begin{cases} ((0.6 - q_l)/2)\tanh(x) + ((0.6 + q_l)/2) & x < 5 \\ -((0.6 - q_r)/2)\tanh(x - 10) + ((0.6 + q_r)/2) & x > 5 \end{cases}. \tag{4.13}$$

The reader might expect this initial condition to approach the traveling wave shown earlier as it has the same far field boundary values, however this is not the case. The traveling wave profile that is approaches is shown in Figure 4.2.

These are not the only possible wave profiles possible with these left and right states. Figure 4.3 shows the result for the following initial condition,

$$q_0(x) = \begin{cases} ((0.6 - q_l)/2)\tanh(x) + ((0.6 + q_l)/2) & x < 10 \\ -((0.6 - q_r)/2)\tanh(x - 20) + ((0.6 + q_r)/2) & x > 10 \end{cases}. \tag{4.14}$$

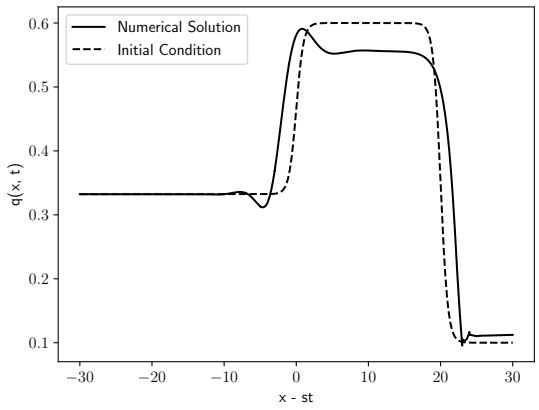

Figure 4.3 Case 2: Multiple Lax Shocks

This initial condition has a larger hump then equation (4.13), and the traveling wave reflects this aspect. In this case the traveling wave is not a steady wave, and there are in fact two shocks. The right shock is an undercompressive shock and the left shock is a traditional compressive shock. Both shocks travel slower than the moving reference frame. They also travel at different speeds from one another so the wave profile changes over time.

4.2.0.3 Case 3: Undercompressive Double Shock

For the left state in the next regime, there is again a unique shock profile for all initial conditions. However this shock profile is not the single Lax shock seen in Case 1. With the following initial conditions,

$$q_0(x) = (\tanh(-x) + 1)\frac{q_l - q_r}{2} + q_r \tag{4.15}$$

where $q_l = 0.4$ and $q_r = 0.1$, figure 4.4 shows a double shock structure. Similar to figure 4.3, we see a undercompressive shock on the right and a Lax shock on the left.

4.2.0.4 Case 4: Rarefaction-Undercompressive Shock

The final traveling wave structure appears when the left state is greater than the undercompressive shock height. In this case we see a rarefaction wave along with the undercompressive shock.

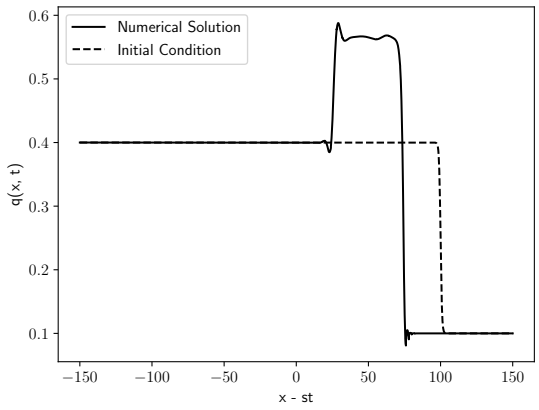

Figure 4.4 Case 3: Undercompressive Double Shock

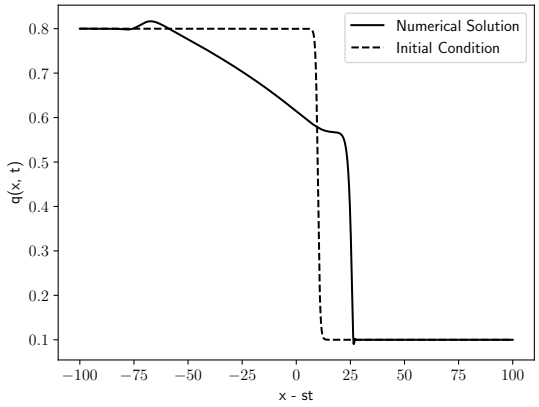

Figure 4.5 Case 4: Rarefaction-undercompressive shock

Figure 4.5 shows the numerical solution for initial condition

$$q_0(x) = (\tanh(-x + 110) + 1)\frac{q_l - q_r}{2} + q_r \tag{4.16}$$

where $q_l = 0.8$ and $q_r = 0.1$. Note that the rarefaction wave and undercompressive shock are traveling at different speeds so they seperate from each other.

Chapter5. Conclusion

This thesis has shown a discontinuous Galerkin method for solving a Thin-Film equation.

The implicit-explicit time-stepping allows for reasonable time steps to be taken given the stiffness of the problem. The nonlinear problem was able to be solved without a Newton iteration. In fact a Picard Iteration was used, and it was demonstrated that only a minimal number of iterations were required to achieve high accuracy. We have demonstrated up to third order accuracy, and this was achieved with the number of Picard iterations less than or equal to the order of accuracy.

BIBLIOGRAPHY

Bibliography